行政院國家科學委員會專題研究計畫 成果報告

P12和其精蟲上受體之分子生殖研究(3/3)

計畫類別：個別型計畫
計畫編號：NSC 91－2311－B－002－049
執行期間：91 年 08 月 01 日 至 92 年 07 月 31 日
執行單位：國立臺灣大學生化科學研究所

計畫主持人：陳義雄

報告類型：完整報告
處理方式：本計畫可公開查詢

中 華 民 國 92 年 10 月 22 日

Distinction of Sperm-binding Site and Reactive Site for Trypsin Inhibition on P12 Secreted from the Accessory Sexual Glands of Male Mice

Ching-Wei Luo[1, 3], Han-Jia Lin[2], S.C.B. Gopinath[2, 4] and Yee-Hsiung Chen[1, 2, *]

[1] Institute of Biochemical Sciences, College of Science, National Taiwan University, Taipei 106, Taiwan, and [2] Institute of Biological Chemistry, Academia Sinica, Taipei 106, Taiwan

[3] Present address: Stanford University School of Medicine, Department of Gynecology and Obstetrics, 300 Pasteur Dr., Room S385, Stanford, CA 94305-5317, USA.

[4] Present address: Functional Nucleic Acids Group, Institute of Molecular and Cell Biology, National Institute of Advanced Industrial Science and Technology (AIST), Tsukuba, Ibaraki 305 8566, Japan

*Correspondence: Dr. Yee-Hsiung Chen; address: P.O. Box 23-106 Taipei, Taiwan; Tel: 886-2-23620261; Fax: 886-2-23635038; E-mail: bc304@gate.sinica.edu.tw

Keywords: Protein structure/Reactive site/Recombinant proteins/Sperm acrosome / Trypsin inhibitor

Running title: Demarcating the active sites on P12 for its multifunction.

ABSTRACT

Six variants of P12, a Kazal-type trypsin inhibitor in the secretion of male mouse accessory sexual glands, were made using single-site mutations including R19L, Y21V, D22G, R43G, K44S, and R45T, based on one-letter-code mutation of amino acids. The other two variants, Nd10 and Cd8, were made using the deletion of 10 and 8 residues from the N- and C-termini, respectively. Their CD profiles revealed maintenance of the P12 conformation in the seven variants excluding Cd8, which became unfolded. Only R19L entirely lost the ability while the other variants were as strong as P12 in inhibiting the trypsin digestion of N-benzoyl-Phe-Val-Arg 7-amido-4-methylcoumarin. The immunocytochemical results demonstrated that D22G and Cd8 failed to bind to sperm, Y21V very weakly did so, and the other variants retained their sperm-binding abilities. Concomitantly, the immunocytochemical stainability of each ligand was parallel to its inhibitory effect on ^{125}I-P12--sperm binding, and a synthetic oligopeptide corresponding to residues 18-24 of P12 was able to inhibit P12-sperm binding. The data together concluded that R^{19} was essential for protease inhibition and D^{22} and/or Y^{21} mainly being responsible for the binding of P12 to sperm. The steric arrangement of R^{19}, Y^{21} and D^{22} on the tertiary structure of P12 is discussed.

INTRODUCTION

Protease inhibitors are ubiquitous in the genital tracts of mammals [1-3]. It is believed that they are important for the protection of genital tract epithelium against the damage of proteolysis [4]. In addition, they have physiological functions in regulating the fertilization processes [5, 6]. For instance, the trypsin-like activity seems to

involve the binding of mouse spermatozoa to zona pellucida [7]. Caltrin is the rat seminal vesicle protein that gives an inhibitory effect on acrosome protease and is able to suppress Ca^{2+} uptake by spermatozoa to prevent premature acrosome reactions far from the oviduct [8, 9]. Hence, the study of protease inhibitors in the genital tract becomes an important subject of molecular reproduction.

The cDNA of P12, a Kazal-type trypsin inhibitor, was cloned from the mouse ventral prostate by Mills et al. [10]. Since P12 RNA message is detectable in the male accessory sexual glands of adult mice while its expression is constitutive in the pancreas [10], substantial progress has been made in establishing its genomic structure. As a result, the DNA-binding sites for some transcription factors such as GC2 and SP1 have been identified in this gene [11, 12]. Meanwhile, we have purified the P12 cDNA-derived protein with an inhibitory constant (Ki) of 0.15 nM to trypsin from mouse seminal vesicle secretions (SVS) [13], and recovered a recombinant P12 with full activity of the naturally occurring P12 from a chimeric polypeptide of glutathione-S-transferase and P12 (GST-P12) expressed in *Escherichia coli* [14]. Moreover, we demonstrated a single-type P12-binding site (1.49×10^6 sites/cell) with a K_d value of 70 nM on the anterior region of mouse sperm, and showed the inhibitory effect of P12 on the Ca^{2+} uptake by mouse sperm [15]. We conducted this study to have a better understanding of the structural feature for multifunction of P12.

Materials and Methods

Purification of P12 and preparation of oligopeptides

Outbred CD-1 mice were purchased from the Charles River Laboratories (Wilmington, Mass, USA) and were maintained and bred in the animal center at the College of Medicine, National Taiwan University. Animals were treated following the

49 institutional guidelines for the care and use of experimental animals. They were
50 housed under controlled lighting (14 h light, 10 h dark) at 21-22 ℃ and were provided
51 with water and NIH 31 laboratory mouse chow *ad libitum*. Adult mice (8-12 weeks
52 old) were humanely killed by cervical dislocation. Seminal vesicles were carefully
53 dissected to free them from the adjacent coagulating glands, and the secretion
54 collected from 50 mice was placed directly into 50 ml of ice-cold 5% acetic acid. P12
55 was purified from SVS according to a previously described procedure [13, 16].
56 The protected oligopeptides were synthesized using stepwise solid-phase
57 methodology on an Applied Biosystems 433A synthesizer with Fmoc chemistry and
58 4-hydroxymethyl phenoxyacetic acid (HMPA) preloaded resin. After each amino acid
59 coupling, an acetylation step was introduced. After cleavage, the crude sample was
60 purified using RP-HPLC on a C18 300A column (Waters prepacked cartridge 2 x 25 x
61 100 mm, 15 μm) with a linear gradient of water and 20% aqueous acetonitrile, both
62 containing 0.1% TFA (v/v), at a flow rate of 20 ml/h. The fractions corresponding to
63 the main peaks were analyzed using RP-HPLC and ES-MS, pooled, and lyophilized.
64 *Preparation of the recombinant P12 variants*
65 For site-directed mutagenesis for P12, we generally followed the instructions of the
66 Promega Altered Sites II *in vitro* Mutagenesis Systems kit (Madison, Wis, USA).
67 Based on P12 cDNA, the mutagenic oligonucleotides used for site-directed
68 mutagenesis included 5'-GGATCATAAATTAGGGGACATCCCGC-3' (R19L), 5'-
69 AGGATCAACAATTCTGGGACAT-3' (Y21V), 5'-CACACAGGACCATAAATT
70 CTGG-3' (D22G), 5'-GCGTTTCCCGTTTTCAAAGC-3' (R43G), 5'-
71 CTCTATGCGACTCCTGTTTTC-3' (K44S), and 5'-
72 GGCTCTATGGTTTTCCTGTTTT-3' (R45T), where the mismatched bases are

underlined, and the mutated proteins are indicated by a one-letter-code mutation of the amino acids in parentheses. The EcoRI/BamHI fragment of P12 cDNA was purified from an expression vector (Gfp), which was previously constructed by the insertion of P12 cDNA into pGEX-2T [14]. The DNA fragment was inserted into pALTER-1. Using single-stranded DNA of the recombinant phagemid DNA as a template, the mutant strand containing each mutagenic oligonucleotide was completed according to the manufacturer's recommendations. The phagemid from each selected transformed colony was sequenced to confirm the mutation. The procedures for construction of two truncated variants were based on PCR amplification. The cDNA of Nd10 in which the N-terminal 10 residues of P12 were deleted or Cd8 in which the C-terminal 8 residues of P12 were deleted was amplified using Gfp as a template and the primer pairs of 5'-CTCGGATCCCATGATGCAGTGGCGG-3' and 5'-CTCGAATTCTCAGCAAGG CCCAC-3' or 5'-CTCGGATCCGCTA AGGT GACTG-3' and 5'-CTCGAATTCTC AGACAGGCTCTATG-3', where the *EcoRI* or *BamHI* site is underlined. The *EcoRI/BamHI* fragment of each P12 variant cDNA was purified and ligated into pGEX-2T, and each constructed vector was transformed into the *E. coli* strain JM109. Expression of the recombinant protein followed a previously described technique [14]. The transformed cells were harvested and resuspended in 10 ml thrombin reaction buffer (50 mM Tris-HCl, 150 mM NaCl and 2 mM $CaCl_2$ at pH 8.0). Cells were then lysed by refreezing them three times in liquid nitrogen and followed by the addition of DNase I. After centrifugation, the supernatant was passed through an affinity column of glutathione agarose beads (Sigma, St. Louis, Mo, USA). According to a method modified from the manufacturer's instructions, the GST fusion protein in the column was mixed with an equal volume of thrombin reaction buffer

97 containing thrombin (20 U/ml) at room temperature for 4 h. The non-bound fractions
98 were eluted from the column, dialyzed against water, lyophilized to dryness, and
99 redissolved in water for the reverse-phase HPLC on a C_4 300A column (Waters,
100 Bedford, Mass, USA). The major sample peak in each chromatogram was identified
101 using SDS/PAGE to be a single 6.0-kDa band that was immunoreactive to rabbit
102 antiserum against P12 using the Western blot procedure (data not shown), which
103 indicated that each P12 variant was purified to homogeneity.
104 *Immunocytochemical staining and binding assay*
105 The rabbit antiserum against P12 was prepared [15]. Mouse spermatozoa were from
106 the caudal epididymis and were prepared according to a method previously described
107 [17, 18]. The spermatozoa were air-dried on a glass slide and fixed with methanol.
108 The slides were washed twice with PBS and preincubated in a blocking solution (3%
109 non-fat skim milk in PBS) for 30 min at room temperature. Cells were further
110 incubated with 10.0 μM P12 or its variant for another 30 min. Alternatively, cells
111 were incubated with each ligand in PBS for 30 min before their fixation on a glass
112 slide for the immunocytochemical analysis. For oligopeptide competition, slides were
113 preincubated with 2.0 mM oligopeptides for 30 min before further incubation in the
114 presence of 10.0 μM P12 for another 30 min. Slides were washed with PBS three
115 times and then immunoreacted with the P12-induced rabbit antiserum diluted 1:200 in
116 the blocking solution for 30 min. Slides were washed three times with PBS to remove
117 excess antibodies before further reacting them with fluorescein-conjugated donkey
118 anti-rabbit IgG (Pharmacia, Sweden) diluted 1:100 in blocking solution for 30 min.
119 All slides were washed with PBS, covered with 50% (v/v) glycerol in PBS, and
120 photographed under a microscope equipped with epifluorescence (AH3-RFCA,

Olympus, Tokyo, Japan).

A method modified from that of Markwell [19] was followed to prepare ^{125}I-P12 according to our method previously used [15]. Spermatozoa (2.5 x 10^6 cells/ml) and 100 nM ^{125}I-P12 in PBS at pH 7.4 were incubated under specified conditions. According to our previously described procedure [20], cells were collected on a Whatman GF/C glass microfiber filter (Whatman, Maidstone, Kent, UK), and the filter was counted with a γ-counter.

Analytical methods and spectral measurement

The kinetic data from the digestion of N-benzoyl-Phe-Val-Arg 7-amido-4-methylcoumarin by bovine pancreatic type III trypsin (Sigma) in the presence of an enzyme inhibitor were analyzed using Dixon's plot to determine the inhibitory constant (*Ki*) of a tightly binding enzyme inhibitor according to a method previously described [13].

Protein concentration was determined using the BCA protein assay (Pierce, Ill, USA) according to the manufacturer's instructions. The homogeneity of the recombinant polypeptide was determined using SDS/PAGE on a gel slab (10.0 x 8.0 x 0.075 cm) according to the method of Laemmli [21]. The proteins on the gel were stained with Coomassie brilliant blue or transferred to a nitrocellulose membrane. After the transfer, protein blots were immunodetected using Western procedures with P12-induced rabbit antisera as the primary antibody and goat anti-rabbit IgG conjugated with horseradish peroxidase (Pharmacia) as the secondary antibody.

The CD spectra were measured with a Jasco J-700 spectropolarimeter under constant flushing with N_2 at room temperature. The mean residue ellipticity, [θ], was

144 estimated from the mean residue weight, which was calculated from the primary
145 structure.

146 The cDNA sequence of each variant was read using the dideoxynucleotide chain
147 termination method with a primer designed for each DNA concerned. Each base was
148 determined at least three times using an ABI PRISM 377-96 DNA sequencer with an
149 ABI PRISM Big Dye Terminator cycle sequencing ready reaction kit (PE Applied
150 Bio-system, Calif, USA).

151 *Molecular Modeling*

152 Following the 'first approach model' reported in the homology-modeling method by
153 Schwede et al. [22], we submitted the amino acid sequence of P12 to the SWISS-
154 MODEL (http://swissmodel.expasy.org/). Template selection, alignment, modeling
155 process, and evaluation were completely automated by the server. The automated
156 modeling procedure started when at least one modeling template was available that
157 had a sequence identity of more than 25% of the P12 sequence. These steps could be
158 iteratively repeated until a satisfying model structure was achieved.

159 **RESULTS**

160 *The tertiary structure of P12*

161 The group of Kazal-type serine protease inhibitors is characterized by a well-
162 preserved amino acid sequence containing three disulfide bridges [23]. Despite that
163 the strict coincidence of the polypeptide chain folding does not occur throughout the
164 inhibitor molecules, their extensive sequence homology suggests a similarity of their
165 overall three-dimensional structures. In the absence of an X-ray structure of P12, we
166 extrapolated a comparative model of its tertiary structure from the homologous
167 modeling using the SWISS-MODEL which automatically selected the known three-

dimensional structures of related family members, including the porcine trypsin inhibitor [24], human pancreatic trypsin inhibitor [25], and pig intestine protease inhibitor [26] as the templates (see Materials and Methods). The high homology of target-template sequences increased the model reliability. According to the molecular model (Figure 1), C^{10}, C^{17}, and C^{25} were respectively cross-linked with C^{39}, C^{36}, and C^{57} in the formation of three disulfide bonds. R^{19}, Y^{21}, D^{22}, R^{43}, K^{44}, R^{45}, R^{52}, and K^{53} were distributed over the entire protein surface. Around 40% of the total amino acid residues formed secondary structures that included one α-helix which stretched from E^{35} to R^{43}, and a small antiparallel β sheet which comprised the three twisted strands of ^{23}PVCG^{26}, ^{27}TDGI^{30}, and ^{53}KGGP^{56}. In addition, there appeared to be a type I reverse turn centered on G^{26} and T^{27}, an irregular reverse turn at the C-terminus of the α-helix where ^{43}RKR^{45} allowed a sharp inversion of the chain path, and a reverse turn at the C-terminal region, which were stabilized by a disulfide bond between C^{25} and C^{57}. The remainder of the molecule may have contained no definite secondary structure. In particular, residues 1-22 may have adopted an extended conformation that stretches across the entire molecule. Homologous alignments of P12 to the known structures of other protease inhibitors suggested that the reactive site for protease inhibition was at the peptide bond between R^{19} and I^{20}, and ^{43}RKR^{45} was the regulatory site for temporary inhibition [27]. It was noted that residues 1-10 of the N-terminal region, ^{43}RKR^{45}, and residues 50-57 of the C-terminal region were three-dimensionally distant from R^{19}, Y^{21} and D^{22} in the loop of residues 17-24.

Protein conformation of P12 variants

Based on the structural features of the molecular model, we prepared eight P12 variants, which were purified to homogeneity (see Materials and Methods). Six were

made from single-site mutations, including R19L, Y21V, D22G, R43G, K44S, and R45T, based on one-letter-code mutations of amino acids. The other two, Nd10 and Cd8, were made by respectively deleting 10 residues of the N-terminus and 8 residues of the C-terminus.

The CD profile of each P12 variant was compared with that of P12 in PBS (Figure 2). The spectra of P12 in the wavelengths of 200-250 nm had two negative bands with magnitudes of -8.1×10^3 and -1.31×10^4 deg•cm^2•dmol^{-1} around 220 nm (band I) and 205 nm (band II), respectively, which suggested a considerable amount of ordered structures including a helix and a mixture of β-forms and β-turns in the P12 molecule, based on the CD spectra of the protein conformation [28-30]. The secondary structure shown in the molecular model of Figure 2 accounts for the characteristic CD. R19L, Y21V, D22G, R43G, K44S, R45T, and Nd10 shared very similar spectra with P12. On the other hand, the protein conformation of Cd8 changed remarkably as evidenced by the disappearance of bands I and II of the native protein and the appearance of a strong negative band below 200 nm, which indicated that Cd8 becomes unfolded. Apparently, the β strand of ^{53}KGGP^{56} is important to maintaining the P12 conformation.

The reactive site for trypsin inhibition and the sperm-binding site on P12

The inhibitory effect of each P12 variant on the hydrolysis of N-benzoyl-Phe-Val-Arg 7-amino-4 methyl coumarin during the course of trypsin digestion was compared with its parent protein (Figure 3). The inhibitory constant (K_i) of each enzyme inhibitor was determined from the kinetic data (Figure 3, top). P12 produced a K_i of 0.15 nM. Except that R19L entirely lost the ability to inhibit the protease, the other variants remained active in protease inhibition. Apparently, R^{19} is indispensable but the N-

terminal 10 residues, Y^{21}, D^{22}, R^{43}, K^{44}, R^{45} and the C-terminal 8 residues are not essential for the protease inhibition.

The sperm-binding ability of each P12 variant was measured. Mouse spermatozoa from the caudal epididymis were incubated with each ligand, and its appearance on the cell surface was examined using an indirect immunofluorescence technique. The cells fixed on a glass slide were incubated with P12 or the cells were incubated with P12 before their fixation on a slide, and no differences in the immunocytochemical patterns were examined. Figure 4 displays the fluorescein fluorescence attributed to each ligand on the cell surface. A crescent fluorescence zone on the anterior region of the head of P12-treated sperm was seen, indicating P12-binding sites on the acrosomal region (Figure 4, row 1). Fluorescence intensity as strong as that of P12-treated cells was visible on the cells preincubated with Nd10 and R19L (Figure 4, rows 2 and 3). Likewise, immunochemical stainability was maintained on cells pretreated with R43G, K44S, or R45T (data not shown). On the other hand, very weak fluorescence on Y21V-treated cells (Figure 4, row 4) and neither D22G nor Cd8 immunochemically stained the sperm acrosome after the cell was preincubated with either variant (Figure 4, rows 5 and 6). P12 barely stained cells after their preincubation with a 200-fold molar excess of G-^{18}PRIYDPV^{24} for 30 min (Figure 5, row 2). Substitution of this oligopeptide with either G-^{11}HDAVAG^{16} or ^{47}EPVLIRKGGP^{56}-G in the cell preincubation did not hinder the binding of P12 to the cell surface (Figure 5, rows 1 and 3). This rules out the sperm-binding site being within these two peptide regions. Meanwhile, ^{125}I-P12 was used for quantitative characterization of the ligand-sperm binding. The sperm-binding ability of each ligand was assayed by its inhibitory effect on the binding of ^{125}I-P12 to the cells. Figure 6

displays data of one representative determination from cell incubation in the presence of 100 nM ^{125}I-P12 and each unlabelled ligand. The IC_{50} determined for each ligand is given at the top of Figure 6. The radiolabelled P12 bound to the cell surface was completely inhibited by unlabelled P12 with an IC_{50} of 98 nM, but was not inhibited by D22G or Cd8 even when a large excess of each ligand to ^{125}I-P12 was present in the cell incubation. Y21V seemed to have very weak sperm-binding ability, because the concentration of up to 10 μM in the cell incubation inhibited less than 40% of ^{125}I-P12-sperm binding. R43G was comparable to P12 in the inhibition of ^{125}I-P12-sperm binding. Nd10, R19L, K44S, and R45T were as strong as P12 in binding sperm. Furthermore, the addition of G^{18}-$PRIYDPV^{24}$ to the cell incubation in a final concentration of 100 μM completely inhibited ^{125}I-P12-sperm binding (data not shown).

DISCUSSION

Our data strongly supported that D^{22} and/or Y^{21} but not R^{19} were responsible for the sperm-binding site, while R^{19} but neither D^{22} nor Y^{21} was indispensable for trypsin inhibition. The sperm-binding site of P12 was not in its C-terminal region, which was found by noting that ^{47}EPVLIRKGGP^{56}G was unable to inhibit P12-sperm binding. This is in line with the fact that Cd8 became unfolded and was unable to bind sperm, which indicates that Y^{21} and D^{22} should be in a conformation which fits them into the P12-binding sites on the sperm head. As shown in the molecular model (Figure 1), the loop of residues 17-24 has a rather certain architecture such that the side chain of R^{19} faces one direction to protrude into the active sites of a trypsin-like protease, while the side chain of either Y^{21} or D^{22} faces another direction. Such a steric restriction for Y^{21}/D^{22} was maintained in R19L, R43G, K44S, and R45T, by noting

that all of these variants shared a very similar CD profile with P12, and they were able to bind sperm. Apparently, the sperm-binding site of P12 did not occur at R^{19}, R^{43}, K^{44}, or K^{45}. The gross conformation of P12 was maintained even when the N-terminal 10 residues were deleted to avoid the formation of a disulfide bond between C^{10} and C^{39}. In fact, Y^{21}/D^{22} in Nd10 retained active sperm binding. This together with the illustration that G-^{11}HDAVAG^{16} was unable to inhibit P12-sperm binding ruled out the sperm-binding site being on the N-terminal 16 residues. On the contrary, the steric requirement for R^{19} in trypsin inhibition was not so rigid that Cd8, which became unfolded, remained active in the protease inhibition.

Winnica et al. reported that excess rat caltrin I or P12 suppressed the proteolytic activity of individual rat or mouse epididymal spermatozoa [9]. This may be a consequence of acrosome inhibition, blockage of proacrosin/acrosin activation, or acrosin release from acrosome. As shown previously [15], P12 is exclusively secreted from male accessory sexual glands and it binds to the plasma membrane overlaying the acrosome. Because acrosin/proacrosin should not be exposed on intact acrosome, the principal acrosomal protease is unlikely to be the P12-binding site on spermatozoal head. More studies are needed to clarify this aspect. Based on the molecular model shown in Figure 1, the binding of D^{22}/Y^{21} on the P12 molecule to its receptor on the sperm head from one direction in the ejaculated semen would turn R^{19} to the other direction. Such a structural feature allows for the binding of a trypsin-like protease from another direction. Therefore, P12 may dissociate from the sperm head when ejaculated spermatozoa encounter a trypsin-like protease in the female reproduction tract under natural circumstance, considering that P12 gave a Ki value of 0.15 nM for the trypsin inhibition and a Kd value of 70 nM for the sperm binding.

288 Determining the way in which P12 and the protease regulates the activity of sperm
289 during their transit in the female reproductive tract is worthy of future study.

290 **ACKNOWLEDGEMENTS**

291 This research was supported in part by grants (NSC91-2311-B001-076 and NSC91-
292 2311-B002-049) from the National Science Council, Taiwan

REFERENCES

1. Fink E, Fritz H. Proteinase inhibitors from guinea pig seminal vesicles. Methods Enzymol 1976; 45: 825-833

2. Fritz H, Tschesche H, Fink E. Proteinase inhibitors from boar seminal plasma. Methods Enzymol 1976; 45: 834-847

3. Meloun B, Cechova D, and Jonakova V. Homologies in the structures of bull seminal plasma acrosin inhibitors and comparison with other homologous proteinase inhibitors of the Kazal typel. Hoppe Seylers Z Physiol Chem 1983; 364: 1665-1670

4. Tschesche H, Wittig B, Decker G, Muller-Esterl W, Fritz H. A new acrosin inhibitor from boar spermatozoa. Eur J Biochem 1982; 126: 99-104

5. Huhtala ML. Demonstration of a new acrosin inhibitor in human seminal plasma. Hoppe Seylers Z Physiol Chem 1984; 365: 819-825

6. Cechova D, Jonakova V. Bull seminal plasma proteinase inhibitors. Methods Enzymol 1981; 80: 792-803

7. Saling PM. Involvement of trypsin-like activity in binding of mouse spermatozoa to zonae pellucidae. Proc Natl Acad Sci U.S.A 1981; 78: 6231-6235

8. Coronel CE, Winnica DE, Novella ML, Lardy HA. Purification, structure, and characterization of caltrin proteins from seminal vesicle of the rat and mouse. J Biol Chem 1992; 267: 20909-20915

9. Winnica DE, Novella ML, Dematteis A, Coronel CE. Trypsin/acrosin inhibitor activity of rat and guinea pig caltrin proteins. Structural and functional studies. Biol Repord 2000; 63: 42-48

10. Mills JS, Needham M, Parker MG. A secretory protease inhibitor requires androgens for its expression in male sex accessory tissues but is expressed constitutively in pancreas. EMBO J 1987; 6: 3711-3717

11. Needham M, Mills JS, Parker MG. Organization and upstream DNA sequence of the mouse protease inhibitor gene. Nucleic Acids Res 1988; 16: 6229

12. Guerin SL, Pothier F, Robidoux S, Gosselin P, Parker MG. Identification of a DNA-binding site for the transcription factor GC2 in the promoter region of the p12 gene and repression of its positive activity by upstream negative regulatory elements. J Biol Chem 1990; 265: 22035-22043

13. Lai ML, Chen SW, Chen YH. Purification and characterization of a trypsin inhibitor from mouse seminal vesicle secretion. Arch Biochem Biophys 1991; 290: 265-271

14. Lai ML, Li SH, Chen YH. Purification and biochemical characterization of a recombinant mouse seminal vesicle trypsin inhibitor produced in *Escherichia coli.* Protein Expr Purif 1994; 5: 22-26

15. Chen LY, Lin YH, Lai ML, Chen YH. Developmental profile of a caltrin-like protease inhibitor, P12, in mouse seminal vesicle and characterization of its binding sites on sperm surface. Biol Reprod 1998; 59: 1498-1505

16. Luo CW, Lin HJ, Chen YH. A novel heat-labile phospholipid-binding protein, SVS VII, in mouse seminal vesicle as a sperm motility enhancer. J Biol Chem 2001; 276: 6913-6921

17. Huang YH, Chu ST, Chen YH. Seminal vesicle autoantigen, a novel phospholipid-binding protein secreted from luminal epithelium of mouse seminal vesicle, exhibits the ability to suppress mouse sperm motility. Biochem J 1999; 343: 241-248

18. Huang YH, Chu ST, Chen YH. A seminal vesicle autoantigen of mouse is able to suppress sperm capacitation-related events stimulated by serum albumin. Biol Reprod 2000; 63: 1562-1566

19. Markwell MA. A new solid-state reagent to iodinate proteins. I. Conditions for the efficient labeling of antiserum. Anal Biochem 1982; 125: 427-432

20. Aarons D, Boettger-Tong H, Holt G, Poirier GR. Acrosome reaction induced by immunoaggregation of a proteinase inhibitor bound to the murine sperm head. Mol Reprod Dev 1991; 30: 258-264

21. Laemmli UK. Cleavage of structural proteins during the assembly of the head of bacteriophage T4. Nature 1970; 227: 680-685

22. Schwede T, Kopp J, Guex N, Peitsch MC. Swiss-model: an automated protein homology-modeling server. Nucleic Acids Res 2003; 31: 3381-3385

23. Laskowski M Jr, Kato I. Protein inhibitors of proteinases. Annu Rev Biochem 1980; 49: 593-626

24. Bolognesi M, Gatti G, Menagatti E, Guarneri M, Marquart M, Papamokos E, Huber R. Three-dimensional structure of the complex between pancreatic secretory trypsin inhibitor (Kazal type) and trypsinogen at 1.8 A resolution. Structure solution, crystallographic refinement and preliminary structural interpretation. J Mol Biol 1982; 162: 839-868

25. Hecht H.J, Szardenings M, Collins J, Schomburg D. Three-dimensional structure of a recombinant variant of human pancreatic secretory trypsin inhibitor (Kazal type). J Mol Biol 1992; 225: 1095-1103

26. Liepinsh E, Berndt KD, Sillard R, Mutt V, Otting G. Solution structure and dynamics of PEC-60, a protein of the Kazal type inhibitor family, determined by nuclear magnetic resonance spectroscopy. J Mol Biol 1994; 239: 137-153

27. Kikuchi N, Nagata K, Shin M, Mitsushima K, Teraoka H, Yoshida N. Site-directed mutagenesis of human pancreatic secretory trypsin inhibitor. J Biochem (Tokyo) 1989; 106: 1059-1063

28. Chen YH, Yang JT, Martinez HM. Determination of the secondary structures of proteins by circular dichroism and optical rotatory dispersion. Biochemistry 1972; 11: 4120-4131

29. Chen YH, Yang JT, Chau KH. Determination of the helix and beta form of proteins in aqueous solution by circular dichroism. Biochemistry 1974; 13: 3350-3359

30. Chang CT, Wu CS, Yang JT. Circular dichroic analysis of protein conformation: inclusion of the beta-turns. Anal Biochem 1978; 91: 13-31

FIGURE LEGENDS

Figure 1. Molecular structure of P12

The tertiary structure was generated by homology modeling, using the automated Swiss-Model service. (A) The amino acid sequence of P12. (B) The tubing diagram shows the polypeptide backbone consisting of one helix (red), one antiparallel β-sheet formed by three short strands (cyan), and other structures (white and gray). In addition, three disulfide bridges (yellow) and ball-and-stick structures for the side chains of R^{19} (brown), Y^{21} (green), and D^{22} (purple) toward different directions are displayed. (C) The space-filling structure depicts the distributions of R^{19}, Y^{21}, D^{22}, R^{43}, K^{44}, R^{45}, R^{52}, and K^{53} on the protein surface. R^{19}, Y^{21}, and D^{22} (red) are distant from the N-terminal 10 residues, ^{43}RKR^{45}, and the C-terminal 8 residues (blue).

Figure 2. Circular dichroism of P12 and its variants

Each protein (0.5 mg/ml) was in PBS at pH 7.4 at room temperature. The spectra of several proteins are selectively represented. Nd10, R19L, Y21V, D22G, R43G, K44S, and R45T share a very similar CD profile with that of P12.

Figure 3. The inhibitory effects of P12 variants on trypsin kinetics

Trypsin at 1.0 nM and each inhibitor at 0-4.0 nM were incubated at room temperature for 3 min before adding the substrate of N-benzoyl-Phe-Val-Arg 7-amino-4 methyl coumarin to a final concentration of 10.0 μM. Hydrolysis of the substrate was measured after 3 min of incubation. The trypsin activity was expressed using the activity measured in the absence of an inhibitor as 100%. Symbols: ●, P12; ○, Nd10; ▼, Y21V; □, D22G; ∇, Cd8; ■, R19L. Except for R19L being unable to inhibit the enzyme, the kinetic data for trypsin activity in the presence of substrate at

5.0, 10.0, and 25.0 μM were analyzed by Dixon's plot to determine the inhibitory constant (K_i, at the top of the figure).

Figure 4. Cytological demonstration for the binding of a ligand to the acrosome of mouse spermatozoa

Mouse spermatozoa prepared from the caudal epididymis were devoid of P12. Freshly prepared cells were dried on glass slides. Slides were incubated with 15 μM of each ligand in PBS for 30 min. The ligand-binding zone on the cell was immunolocalized by an indirect immunobfluorescence method using rabbit antiserum against P12 and fluorescein-conjugated anti-rabbit IgG. Slides were observed using a fluorescence microscope (A) or a light microscope (B). Bar = 10 μm.

Figure 5. Cytological examination of the inhibitory effects of oligopeptides on P12-sperm binding

Freshly prepared spermatozoa on glass slides were preincubated with 2.0 mM of G-^{11}HDAVAG^{16} (row 1), G-^{18}PRIYDPV^{24} (row 2), or ^{47}EPVLIRKGGP^{56}-G (row 3) in PBS for 30 min at room temperature before the addition of P12 to a final concentration of 10.0 μM in the cell incubation, which proceeded for another 30 min. The P12-binding zone on the cell was immunodetected as described in Figure 5. Slides were observed using a fluorescence microscope (A) or a light microscope (B). Bar = 10 μm.

Figure 6. Inhibition of ^{125}I-P12-sperm binding by P12 variants

Spermatozoa (2.5 x 10^6 cells/ml) in PBS were incubated for 1 h in the presence of 100 nM ^{125}I-P12 and 0-10 μM P12 or its variant at room temperature. Radioactivity associated with the cells was measured (see text for details). Results are expressed as percentages of counts measured in the absence of unlabelled ligands. Points are the mean of three determinations. The S.D. of each point is less than 5%. Symbols: ●, P12; ○, Nd10; ▼, Y21V; □, D22G; ∇, Cd8; ■, R19L. Y21V showed very weak ability, while D22G and Cd8 failed to inhibit the binding of ^{125}I-P12 to sperm. The IC_{50} of each P12 variant was computed using a Cricket Graph and is listed at the top of the figure.

(A)

```
1         10        20        30
|         |         |         |
AKVTGKEASCHDAVAGCPRIYDPVCGTDGI

31        40        50        57
|         |         |         |
TYANECVLCFENRKRIEPVLIRKGGPC
```

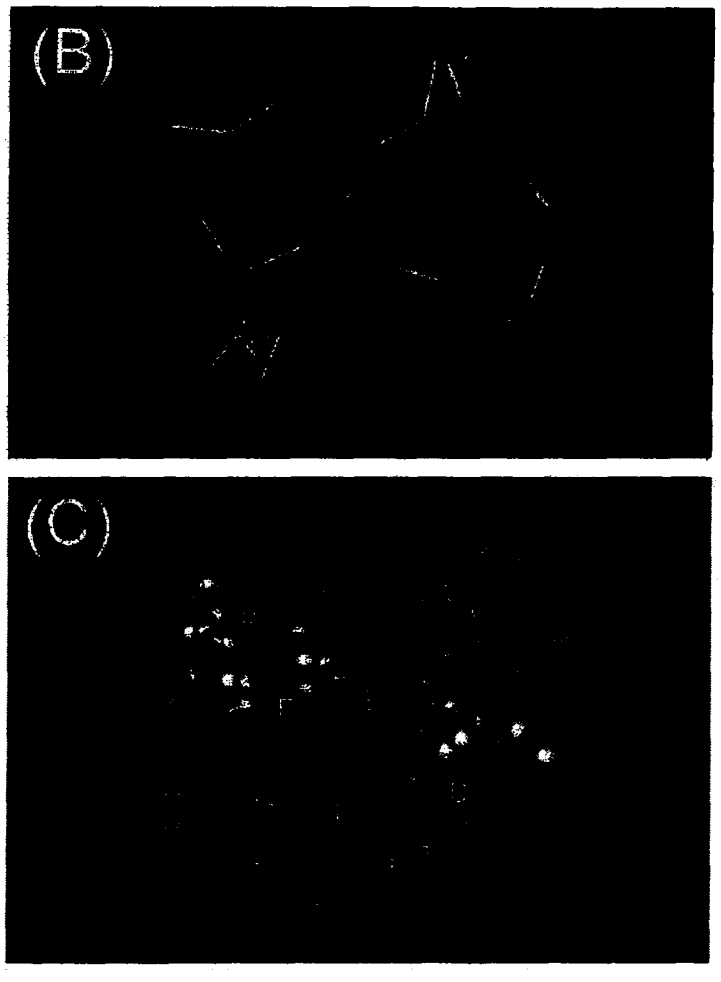

Figure 1

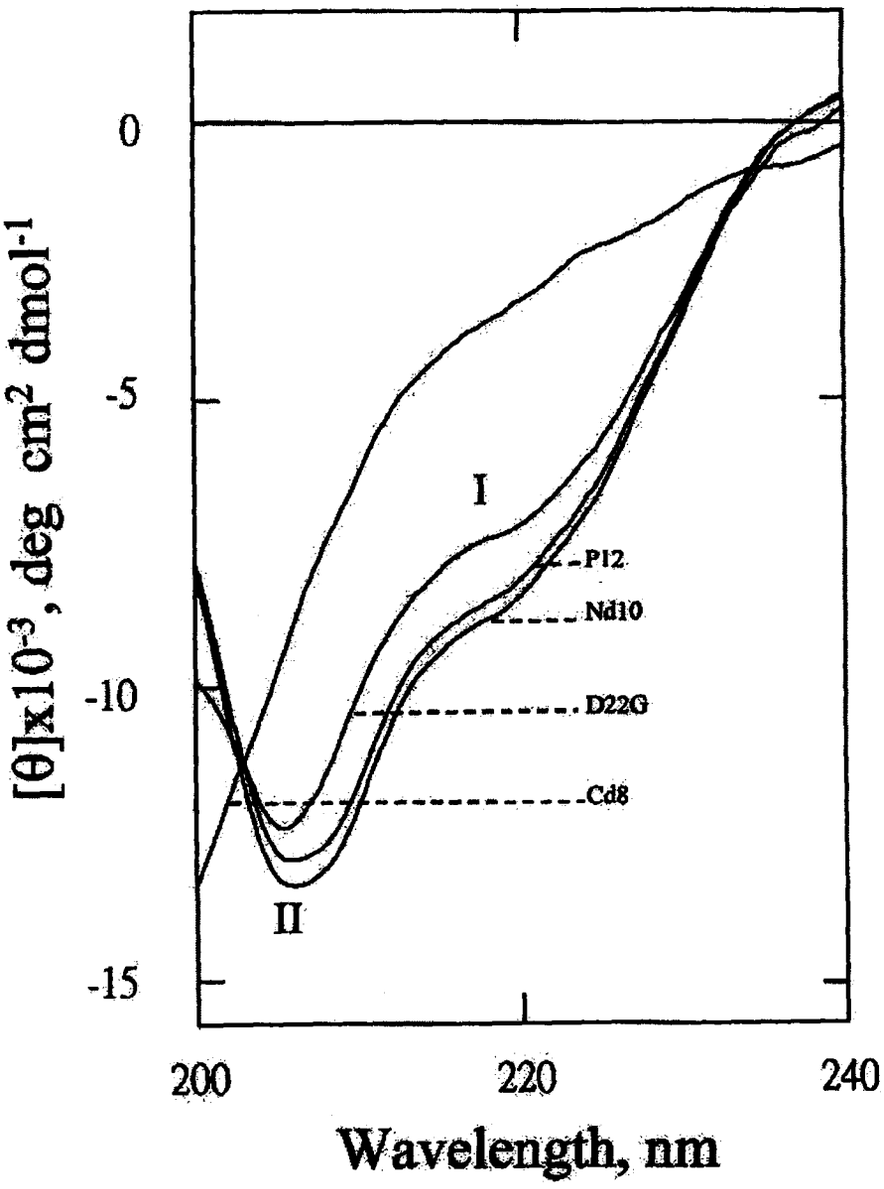
0
-5
-10
-15
200
220
240
[θ]x10-3, deg cm2 dmol-1
Wavelength, nm
I
II
PI2
Nd10
D22G
Cd8

Figure 2

Inhibitor	Ki (nM)
P12	0.15
N_d10	0.17
Y21V	0.19
D22G	0.28
R19L	—
R43G	0.14
K44S	0.13
R45T	0.16
C_d8	0.28

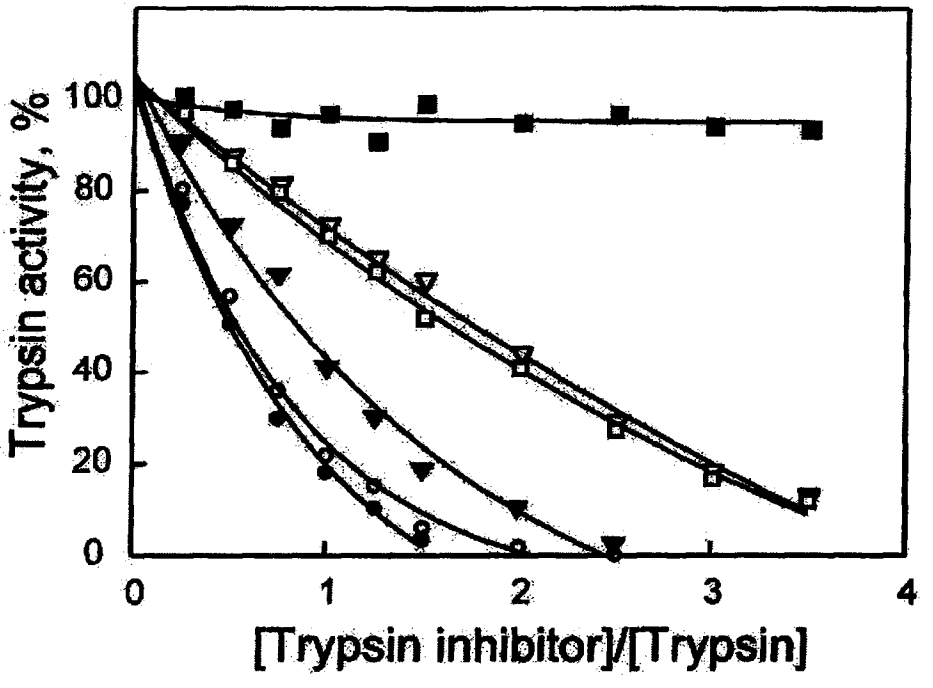

Figure 3

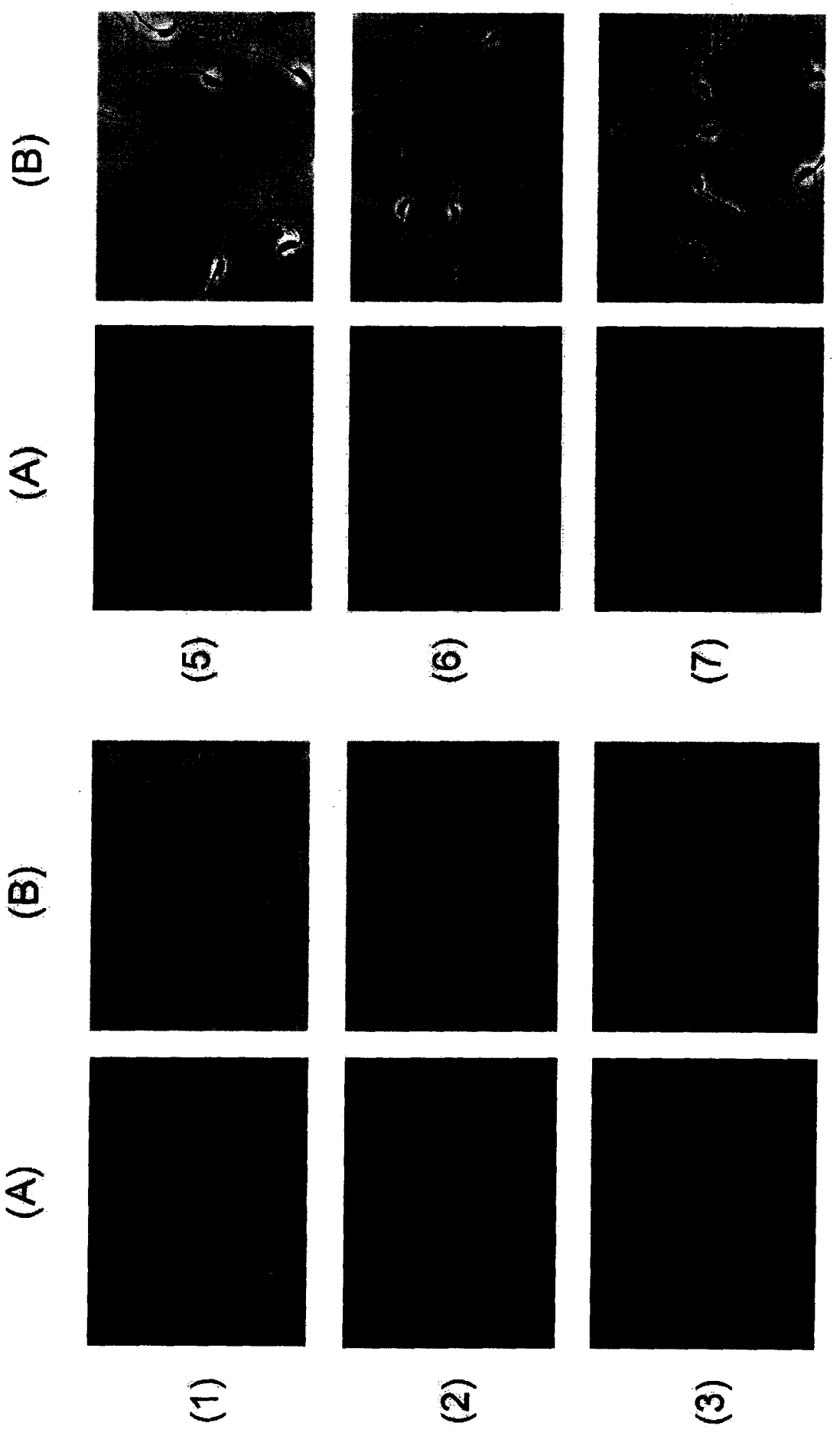

Figure 4

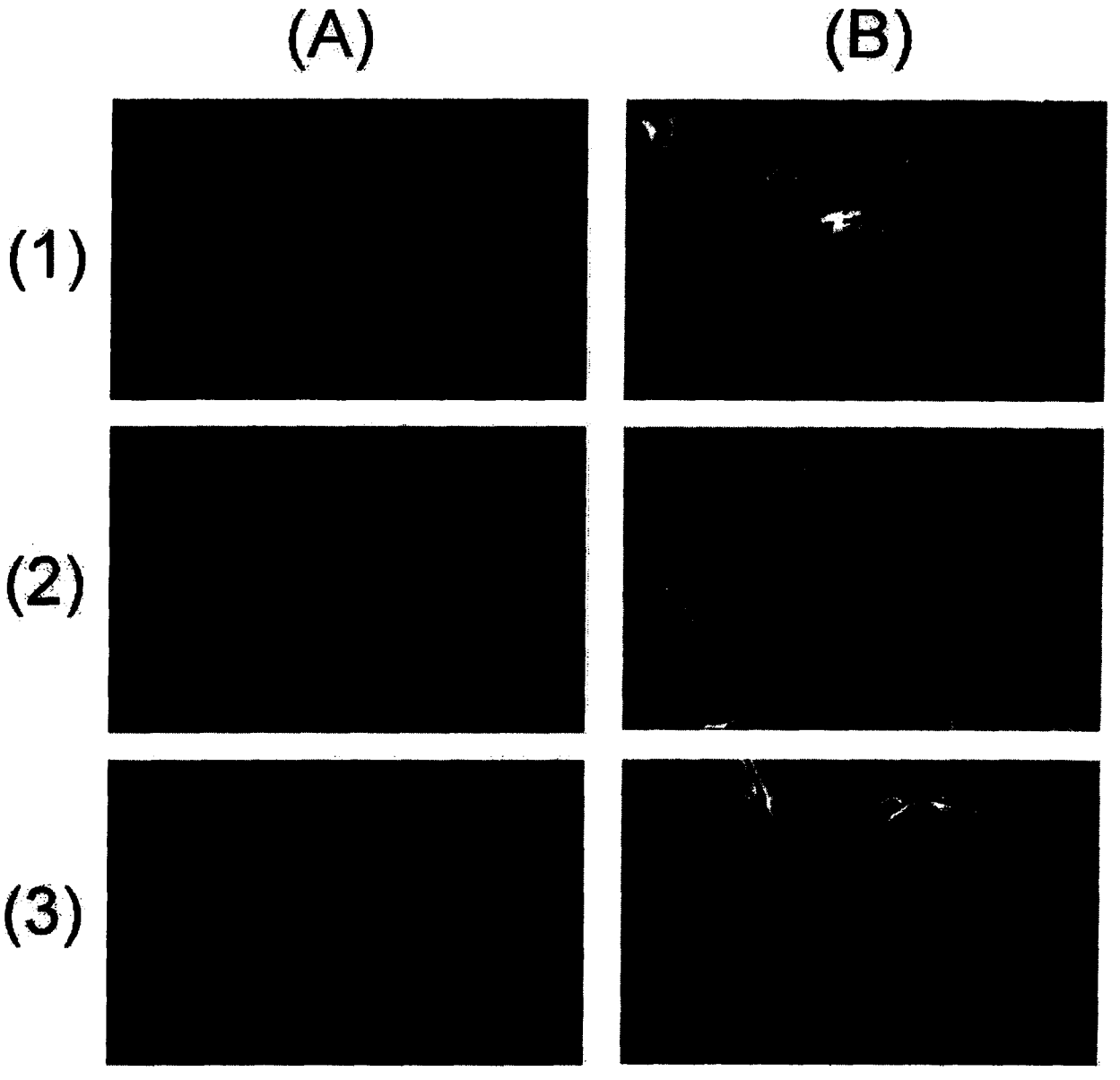

Figure 5

Protein	IC_{50} (nM)
P12	98
Nd10	75
R19L	106
Y21V	—
D22G	—
R43G	158
K44S	79
R45T	102
Cd8	—

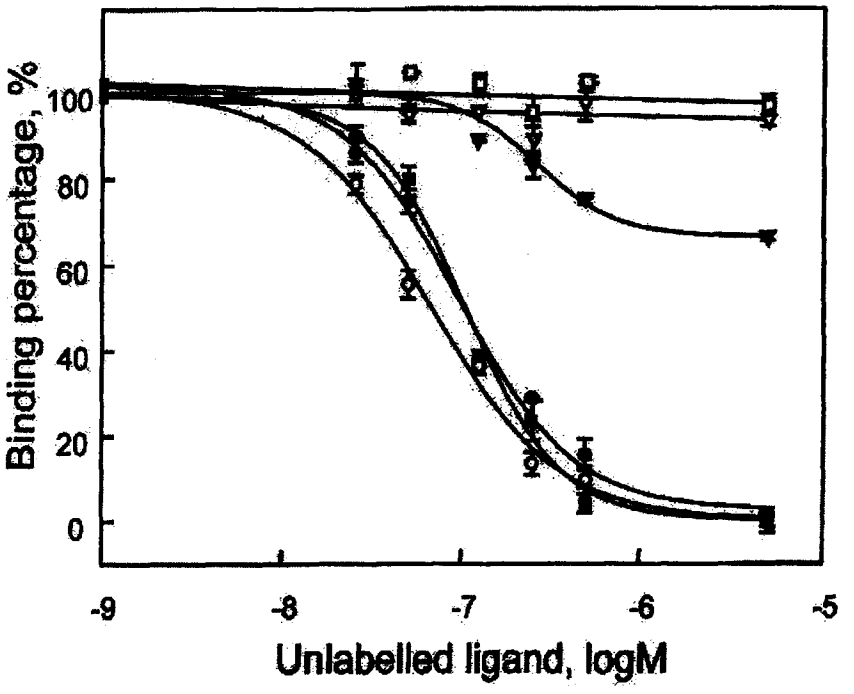

Figure 6